Prospects of Using a Pulsed Electrostatic Tractor With Nominal Geosynchronous Conditions

Joseph Hughes and Hanspeter Schaub

***Abstract*— The geosynchronous (GEO) orbital regime is becoming cluttered with derelict space debris, which raises the collision risk for satellites in a very valuable orbit. Touchless reorbiting options have been proposed for moving this debris to a graveyard orbit to avoid the risk of physically docking with large, multiton defunct satellites that can be tumbling at several degrees per second. This paper investigates the electrostatic tractor (ET), which uses an electron beam mounted on a tug spacecraft to irradiate a passive debris object. The tug quickly rises to a positive steady-state voltage, and the debris quickly falls to a negative steady-state voltage to create an attractive tugging force. The tug maintains a fixed relative position during the reorbit using inertial thrusting. The Coulomb force can be used as a means of touchless actuation for geosynchronous debris reorbiting, detumbling, and formation flying. This paper investigates the prospects of using a beam with pulsed current. The off-pulsing periods can have benefits for sensing and thrusting applications, and the pulsing charging can lead to higher force levels for the same electrical power used in particular conditions. A Monte Carlo analysis is performed to study the mean electrostatic force, considering a range of beam currents, voltages, pulsing duties cycles, and vehicle sizes. Power-limited regions are identified where the pulsed tractor has a magnitude that is comparable or greater than the mean continuous beam force. This creates interesting alternate methods to implement an ET while having periodic off periods. The tractor performance is illustrated through the debris reorbiting scenario. A detailed equal power analysis determines that even duties cycles as low as 10%–20% can lead to forces comparable to the continuous beam performance, or even do better for some powers.**

***Index Terms*— Electrostatic tractor, orbital debris, re-orbiting.**

I. Introduction

THE geosynchronous (GEO) orbit regime is home to at least U.S. $18.3 billion in space assets from the civil, commercial, and defense sectors [1]. Of the 1369 tracked objects in GEO, only 21% are controlled. This crowding of large, tumbling, often school-bus-sized objects creates the probability of collision, which is expected to worsen with current launch and reorbiting trends [2].

To reduce the collision probability, many concepts have been proposed to move GEO debris into a graveyard orbit about 200–250 km above GEO. Some of these require physical contact with the debris object, such as harpoons, nets, and robotic arms [3]. These methods are attractive, because once contact is made, the tug spacecraft can use its thrusters to reorbit the debris object in only a few orbits. The docking process is very challenging and raises strong concerns regarding colliding with the debris and creating more debris. In addition, the robotic docking solutions discussed in [4] require that the debris be rotating at rates under 1°/s. However, many uncontrolled debris objects spin up to many tens of degrees per second [5]. Because of this, methods are being investigated to despin the debris before grappling or touchless tugging solutions are required.

Touchless tugging concepts are more simplistic in that they do not require grappling and are safer in that they reduce the risk of collisions. However, they typically require longer reorbiting times. The ion beam shepherd [6], [7], for example, uses a beam of ions to push the debris ahead of the tug. The tug must have an additional thruster that has at least twice the thrust of the ion beam. Another concept is the electrostatic tractor (ET) [8]–[10], which uses an electron beam to charge a tug spacecraft positive and a debris object negative. An attractive Coulomb force results from this charging. For two moderately sized spacecraft (3-m diameter) charged at ±20 kV, and separated by seven craft radii, the debris feels a 1.2-mN force that could raise its orbit by more than 5 km/day [11]. A tug craft equipped with an electron gun and low thrust motors could move defunct GEO satellites to a graveyard orbit in a matter of 1–3 months [11]. In addition, spacecraft with nonsymmetric charge distributions will also feel and apply torques through this charging [12]–[14]. This torque can be used to touchlessly detumble noncooperative space objects in a matter of days [15] depending on the debris inertia and spin rate.

Charging to the needed levels is feasible, as spacecraft naturally charge to tens of kilovolts in eclipse GEO conditions [16] and have used charge emission devices to control their own potential [17]. Interactions between this charge and the Earth's magnetic field can cause perturbations especially for high-area-to-mass-ratio objects [18], [19]. With active charging, these perturbations can be harnessed for orbit changes by pushing off the earth's magnetic field [20]–[22] rather than from using chemical propellant.

While prior work on the ET performance focuses on a continuous charge emission from the tug [11], [23], [24], this paper augments the ET concept by using a pulsed electron beam rather than a continuous one, as is shown in Fig. 1. Of interest is under what conditions the pulsed charging leads to tractor forces levels that are comparable or greater than the continuous charging case.

Manuscript received July 27, 2016; revised December 19, 2016 and February 22, 2017; accepted March 13, 2017. Date of publication March 29, 2017; date of current version August 9, 2017. *(Corresponding author: Joseph Hughes.)*

The authors are with the University of Colorado Boulder, Boulder, CO 80309-0401 USA (e-mail: joseph.hughes@colorado.edu; hanspeter.schaub@colorado.edu).

Color versions of one or more of the figures in this paper are available online at http://ieeexplore.ieee.org.

Digital Object Identifier 10.1109/TPS.2017.2684621

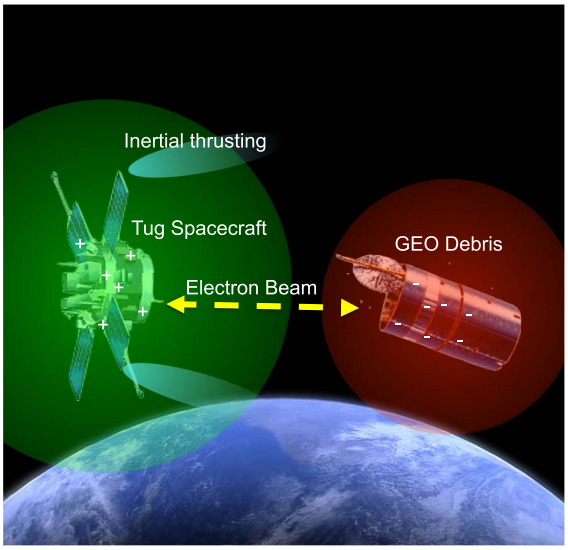

Fig. 1. ET allows spacecraft to touchlessly exert forces and torques on passive space objects.

The physical explanation of the average pulsed force being higher than the continuous force for equal power is that the average pulsed force is decreased linearly by the duty cycle but increased quadratically. As an example, consider two equal power beams applied in a vacuum, one continuous and one pulsed at a 50% duty cycle. Since the pulsed beam is only running half the time, it can draw twice the power in the time that it is ON. If it uses this extra power to double the voltage, it can double the charge stored on each craft. Since the force is roughly proportional to the product of the two charges, it will increase by a factor of 4 while the beam is ON, and decay to zero in other half of the time. This results in an average force that is more than twice the continuous force in this simple vacuum case. However, in a plasma, the situation is more complex. The current required to achieve a potential is increased at higher voltages to offset the increased current from the plasma. Furthermore, it takes some time for the large space objects to charge to their steady-state values. In contrast to the earlier continuous beam ET studies, the time-varying charging equations must be considered. The result is a complex set of competing conditions, which are investigated in this paper.

To investigate the entire search space, a Monte Carlo analysis is first used, varying a broad range or spacecraft and electron beam parameters. This numerical analysis tool provides broad insights into the electrostatic force and reorbiting behavior avoiding assumptions about optimality. For the scope of this paper, a fixed set of nominal GEO space weather conditions are modeled. Of interest is under what conditions pulsing can lead to interesting solutions where the objects are only charged for part of the time while retaining or even improving the tugging performance. Next, a deterministic equal power analysis is performed about a nominal continuous case. This analysis is then repeated at different power levels.

II. Problem Statement

The goal of this paper is to investigate trends and benefits of pulsed charging for the ET from a force magnitude and off-period consideration. As a simplifying assumption, this analysis considers two aluminum spheres in quiet GEO plasma. In reality, many GEO spacecraft are not perfectly conducting, and have complex geometries. The plasma environment at GEO is also typified by many different temperature populations of plasma [25]. This paper focuses on a fixed, nominal space weather condition to focus on the impact of a broad range of electron beam and spacecraft parameters. Considering high energy space weather storm events introduces a significant complexity, as illustrated in [24] for the continuous charge case, and is left for future work.

A. Space Weather and Material Dependence

Spacecraft charging, with or without a beam, is dependent on the space weather parameters, such as the electron and ion temperatures (T_e, T_i), and electron and ion density (n_e, n_i). These space weather parameters vary with solar cycle, local time, and K_p index [25]. However, these changes only modulate the performance of the continuous ET at the 20% level [24]. In this analysis, quiet ($K_p = 1.5$) afternoon ($LT = 15{:}00$) values are used for electron densities and temperatures. There are two major populations of ions at GEO, one cold (10–100 eV) and dense ($n_i \sim 10$ cm^{-3}) and the other tenuous ($n \sim 1$ cm^{-3}) and hot ($kT_i \sim 10$ keV) [26]. Especially, for a very negative spacecraft, the cold ions contribute much more current than the hot ions; thus, the hot ions are not included.

Further analysis is required to ascertain the effect of solar cycle on reorbiting performance. The nominal GEO space weather assumption provides an initial assessment of how the pulsed ET will perform in a mission scenario. Solar storms, which cause high K_p values, are short lived compared with the deorbiting time (months) and are expected to play a small role in the overall performance. As these events cause natural charging, earlier work found that for the continuous beam ET case, the storm conditions made it easier to reach the desired potential levels [24].

A highly charged spacecraft has an impact on the local plasma environment. However, as the nominal GEO conditions have an ion Debye length of around 16 m and an electron Debye length of around 320 m, and we are flying spacecraft dozens of meters apart, this impact is relatively small on the electrostatic force studies in this paper. Detailed understanding of spacecraft charging with a high voltage and current electron beam for two nearby spacecraft in a dipole sheath is a complex problem. The simplified charging model employed in this paper is sufficient for a basic analysis of the expected pulsed ET performance.

This paper assumes that the spacecraft are conductors and spherical in shape. This is a good assumption for many GEO spacecraft as they are built with a generally conducting outer surface to avoid differential charging. The shape assumption is a reasonable first step for this early study as the electric fields approach that of a sphere as the separation distance increases. For nonspherical spacecraft, the attitude influences which spacecraft surfaces are sunlit, which will effect the charging. Including dielectric materials in the future work

TABLE I
NOMINAL GEO SPACE WEATHER PARAMETERS AND APPROXIMATE MATERIAL PROPERTY VALUES

Parameter	Value
j_{ph}	20 μA/m^2
$k_{\text{B}}T_{\text{ph}}$	2 eV
n_{e}	0.7 cm^{-3}
n_{i}	11 cm^{-3}
$k_{\text{B}}T_{\text{e}}$	1300 eV
$k_{\text{B}}T_{\text{i}}$	50 eV
E_{Me}	400 eV
δ_{M}	2
β	1.36 keV$^{-1/2}$
E_{Mi}	40 keV

on the exterior with varying secondary electron yield and backscattering properties as well as bulk conductivities also effects the ET performance.

A detailed description of the charging model is given in the Appendix. The model includes plasma charge flux onto the spacecraft, electron backscattering, electron and ion-induced secondary electron emissions (SEEs), the tug's electron beam itself, and the photoelectron currents. The models used for SEE via incident electrons, electron backscattering, and SEE via incident ions are those proposed by Lin and Joy [27] and the Nascap Scientific Documentation [28], respectively. Experimental values for the SEE material parameters can vary by more than a factor of 6 [27], which adds uncertainty to charging. Further analysis is needed to investigate the robustness of these findings to variability in SEE model parameters.

Hogan and Schaub [29] used Denton *et al.*'s [25] results to approximate the charging environment using only one population of ions and electrons. The same environmental model is used in this analysis and the parameters are shown in Table I. All variables are defined in the Appendix.

B. Position-Dependent Capacitance

All of the charging currents are the functions of voltage, not charge. Since the currents directly change the charge of each craft, not the voltage, a mapping between voltage and charge is needed. The voltage of each spacecraft is a function of its own charge and the charge of nearby spacecraft. If one assumes two spherical spacecraft separated by ρ, which is much larger than the debris and tug spacecraft radii R_D, R_T, the relation becomes [30]

$$\begin{bmatrix}\phi_T\\ \phi_D\end{bmatrix} = \frac{1}{4\pi\epsilon_0}\begin{bmatrix}1/R_T & 1/\rho\\ 1/\rho & 1/R_D\end{bmatrix}\begin{bmatrix}q_T\\ q_D\end{bmatrix}. \tag{1}$$

Here, ϕ_T and ϕ_D are the absolute potentials and R_T, R_D are the effective radii of the tug and debris, respectively. This relationship is used at each time step to calculate the voltages, which are then used to calculate the currents.

C. Force Model

The force between two point charges separated by ρ is given by [31]

$$\boldsymbol{F} = \frac{q_D\, q_T}{4\pi\epsilon_0\rho^2}\hat{\boldsymbol{\rho}}. \tag{2}$$

In a plasma, Debye shielding will lessen this force. In many cases, this force reduction will be small, because even though the ion Debye length is comparable to the separation, the spacecraft voltages are much higher than the plasma temperatures. This leads to a stronger force than would be predicted using standard Debye shielding formulation [32], [33]. In this analysis, space charge shielding is ignored and the Coulomb force law is used.

For the pulsed ET, the pulsing frequency is on the order of Hz, which is much faster than the spacecraft orbital period of 24 h. This allows us to treat the average force as continuous for the purposes of orbit raising.

III. METHODS

A. Time-Varying Charge Evaluation

A numerical simulation is developed to find the currents as a function of both the spacecraft charge levels and time. This is used to propagate the charge on the tug and debris spacecraft $[q_T, q_D]^T$ through time using an RK4 integrator. This is shown explicitly as follows:

$$\begin{bmatrix}\dot{q}_T\\ \dot{q}_D\end{bmatrix} = \begin{bmatrix}\sum I_T(q_T, q_D, t)\\ \sum I_D(q_T, q_D, t)\end{bmatrix}. \tag{3}$$

Auxiliary variables of $\boldsymbol{\phi}(t) = [\phi_T(t), \phi_D(t)]^T$ and $F(t)$ are also recorded.

B. Pulsed Beaming Monte Carlo Analysis

In this analysis, the pulsed beam is modeled by a square wave, which has four parameters: voltage (V_b), current (I_b), period (T_p), and duty cycle (d). Varying the tug (R_T) and debris (R_D) radii increases the search space to six independent parameters.

The four parameters that apply to both pulsed and continuous beams (R_T, R_D, I_b, and V_b) are chosen randomly within the bounds shown in Table II. This parameter set is enough to specify the continuous beam properties. For the pulsed beam, two additional beam parameters are required to be chosen: T_p and d. Both the continuous and pulsed parameter sets are then fed into the integrator described earlier. The average force in the case of the pulsed beams and the force at the final time step, where both craft have achieved their steady-state voltages for the continuous cases, is computed for each run and stored in a master file along with the parameters that produced it.

The radii range has been chosen to match the self-capacitance of typical GEO spacecraft [34] (100–600 pF). The beam voltage extends up to 100 kV, which is higher than currently flown spacecraft electron guns of 20–40 kV. However, the Beam Experiment Aboard Rocket mission demonstrated a 1-MeV accelerator for ions in space [35], [36]. With a 100-kV beam, each spacecraft would

TABLE II
MONTE CARLO BOUNDS

Parameter	Lower Limit	Upper Limit
R_T	1.5 m	5m
R_D	1.5 m	5m
V_b	5 kV	100 kV
I_b	0.1 mA	20 mA
T_p	0.1 s	1 s
d	0.01	0.99

ideally charge to ±50 kV in a vacuum and neglecting SEE and backscattering. With these kilovolts of potentials, it is critical that all outer surfaces of the tug are electrically connected to avoid differential charging and arcing. In addition, the high energy electrons may cause harmful bremsstrahlung radiation [37], which could damage spacecraft electronics [17]. In these simulation scenarios, the beam current is designed to overwhelm environmental currents, and the pulse period is chosen to be longer than typical spacecraft charging times. The duty cycle ranges from 1% to 99%.

A center-to-center distance r of $5(R_T + R_D)$ is used. This gives four craft diameters of standoff distance (12–40 m). Since many GEO spacecraft have large solar panels and may be rotating, even this distance will require very careful autonomous formation flying. This is not outside the realm of feasibility considering the evolving structured light and LIDAR-based relative motion sensing systems being developed [38]. The PRISMA mission demonstrated cooperative controlled formation flying as close as 5 m [39]. The ANGELS mission also demonstrated close noncooperative formation flying, but has not publicly released a minimum distance.

The simulation integration time is constrained to be the larger of ten pulse periods or 0.1 s. The time step is chosen so that either there are 50 steps in the "on" segment of the period, or that the norm of the largest possible currents cannot change either craft voltage by more than 5 kV during one time step. The 20 000 runs were computed, 10 000 for the pulsed ET and 10 000 for the continuous ET.

IV. MONTE CARLO-BASED FORCE ANALYSIS

This section presents the results of a Monte Carlo analysis of the simulation parameters discussed in Section III-B. This numerical approach has the advantage that no *a priori* assumption is being made on what constituted a good set of simulation examples. The results provide a broad overview of the ET force behavior.

The average force produced by a pulsed beam is plotted against the steady-state force of a continuous beam in Fig. 2 as black dots. Points below the solid line with slope equal to 1 represent parameter sets (R_T, R_D, V_b, I_b, T_p, and d) where the average force was higher for the continuous beam (setting d equal to 1). In this plot, the continuous beams always use more power, and typically produce more force.

There are far more points below the line than above it, which is expected, since the pulsed beam is expected to increase force

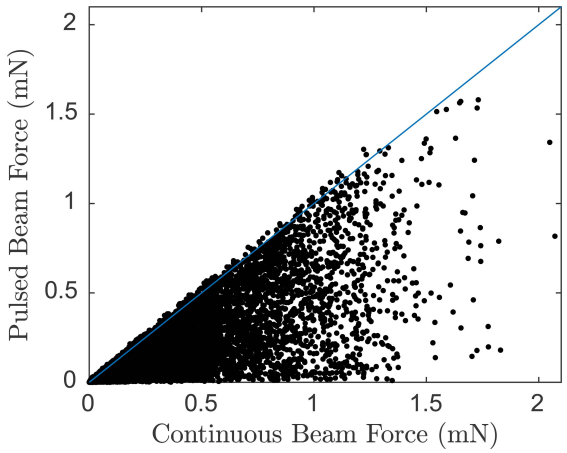

Fig. 2. Comparison of forces produced by continuous and pulsed beams with all other parameters equal.

efficiency, not pure force. However, many of these pulsed cases open up large (hundreds of milliseconds) windows where both spacecraft are not charged and the beam is OFF during which measurements and thrusting can happen without interference.

As for the magnitude of the continuous forces, there are improvements over prior work. There are multiple parameter sets that produced forces larger than 1.5 mN; in contrast, Hogan [23] found forces less than 1 mN, but used a more conservative beam voltage and a different charging model.

The pulsed ET begins to show force increases compared with a continuous ET if a power-limited tug is considered. The power in the beam can be expressed as $P = V_b I_b$ for the continuous case, and $P = d I_b V_b$ for the pulsed beam. In reality, the electrical load on the spacecraft will exceed this value. Many components of a pulsed electron beam require constant power, so the efficiency for the pulsed beams is likely lower than this analysis shows.

Both the average force (for the pulsed cases) and the steady-state force (for a continuous cases) are plotted against the power in the beam in Fig. 3. The blue points represent continuous beam cases, and the red points represent pulsed cases. This plot shows the force efficiency increases of a pulsed ET. The efficiency is found by taking the ratio of the force (y-axis) to the power in the beam (x-axis). Points at the top of the scatter cloud represent the most force produced at that power level. As can be seen in the zoomed-in figure, the highest points are red more often than they are blue, which means that a pulsed beam produces more force for a given power inside the power band of 10–50 W. This trend disappears for high powers due to the 100-kV cap on beam voltage.

Some tug spacecraft may have limited electron beam voltage rather than electron beam power. At sufficiently high voltages, sharp corners on either spacecraft may arc into the ambient plasma through coronal discharge. A high energy beam may also cause bremsstrahlung, where the deceleration of an electron releases X-rays that could seriously damage spacecraft electronics. Fig. 4 shows the force produced by a beam of a given voltage. Blue once again represents continuous cases while red represents pulsed cases.

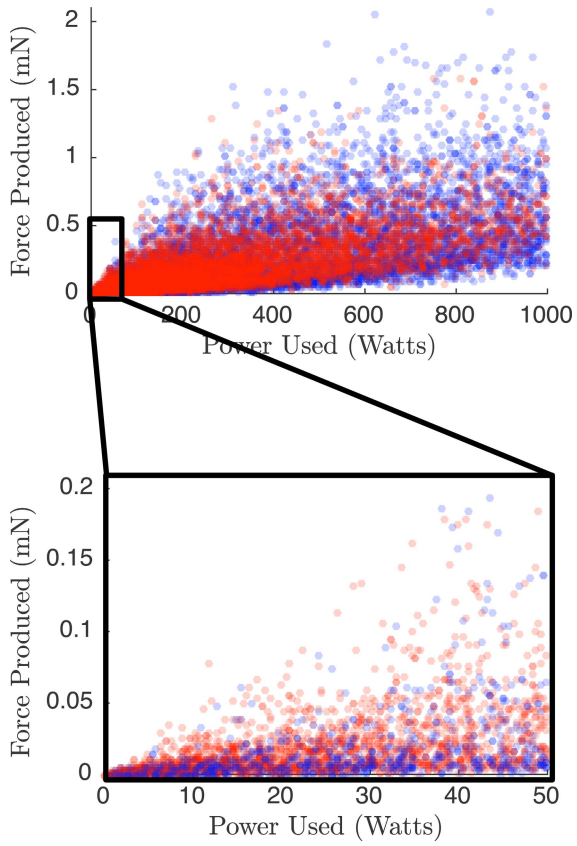

Fig. 3. Comparison of force produced by continuous (blue) and pulsed (red) beams plotted agains the power in the beam.

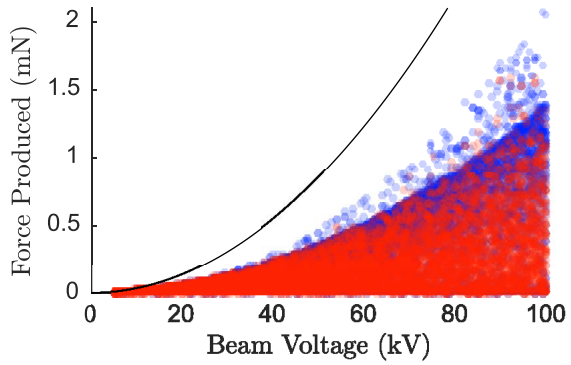

Fig. 4. Comparison of force produced by continuous (blue) and pulsed (red) beams plotted agains the voltage of the beam. The theoretical max is shown as a solid black line.

This voltage-limited case contrasts the power-limited case of Fig. 3 in that the continuous beam always produces more force. This can be seen by the higher concentration of blue points near the upper maximum line. Figs. 3 and 4 show how pulsed beams produce more force in some power-limited situations while continuous beams produce more force in voltage-limited situations.

There is a very strong quadratic limit in the maximum force that can be produced for a given voltage. This matches the findings of Schaub and Sternovsky [11] that the maximum force between two equal-radius charged spherical spacecraft in vacuum that employ an electron gun with accelerating voltage of V is

$$F_{\max} = \frac{4\pi\epsilon_0 R_T R_D}{(r - R_T)(r - R_D)} \frac{V^2}{4} \tag{4}$$

where the spacecraft are separated by r. For our analysis, the center-to-center separation $r = 5(R_D + R_T)$ is used. Inserting this yields

$$F_{\max} = \frac{4\pi\epsilon_0 R_T R_D}{80R_T^2 + 164R_T R_D + 80R_D^2} V^2. \tag{5}$$

The maximum of this force occurs when the craft are equally sized, but is independent of the actual sizes. This is only because small craft are closer together. Using equally sized spacecraft yields

$$F < \frac{4\pi\epsilon_0}{324} V^2 \tag{6}$$

$$F < \left(3.434 * 10^{-4} \frac{\text{mN}}{\text{kV}^2}\right) V^2. \tag{7}$$

For a 100-kV beam, the theoretical maximum is 3.43 mN. This theoretical maximum is also shown in Fig. 4 as a solid black line and can be seen to bound all data points. The data points seem to be bounded by an even shallower parabola. The electron beam will cease to achieve charge transfer when $\delta + \eta > 1$, which will happen when the landing energy is low. This is one of many effects that prohibit achieving the theoretical maximum force.

V. Reorbiting Analysis

An end objective of the ET includes reorbiting debris to a graveyard orbit, some 250–300 km above GEO. This process is mathematically modeled as a perturbation in the along-track direction, which slowly changes the semimajor axis of the debris orbit. Schaub and Jasper [34] approximated the change in semimajor axis over 1 day as

$$\Delta a = \frac{4\pi}{n^2} \frac{F}{m} \tag{8}$$

where n is the mean motion of the orbit [radians/second]. They went on to find this linear relationship between the effective radius (for capacitance matching) and launch mass

$$m = \frac{R - 1.152 \text{ m}}{\left(0.00066350 \frac{\text{m}}{\text{kg}}\right)} \tag{9}$$

where the radius is between 1 and 6 m, where it predicts masses between 1000 and 6000 kg. The launch mass is a conservative estimate of the actual mass as all of the station-keeping propellant is likely exhausted. The tug is assumed to be able to keep up with the maximum acceleration of the debris using thrusters. The SMA rate is then found by using the debris mass. The SMA rate is plotted against the power in the beam for both the pulsed and continuous beam cases in Fig. 5 where red points are pulsed and blue points are continuous.

Again, red points outnumber blue points at the upper edge of the scatter cloud in the lower zoomed-in plot. This means that in power-limited cases, a pulsed beam will achieve higher

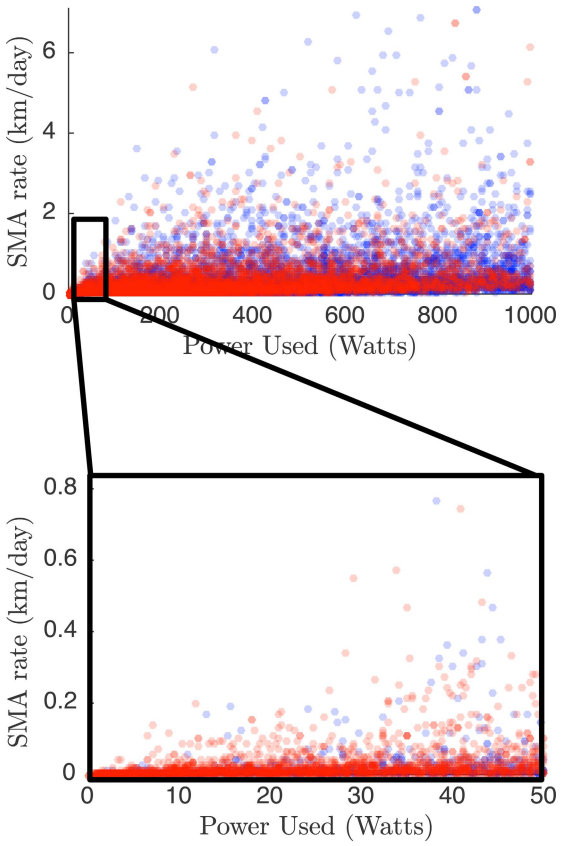

Fig. 5. Comparison of SMA rate produced by continuous (blue) and pulsed (red) beams plotted agains the power in the beam.

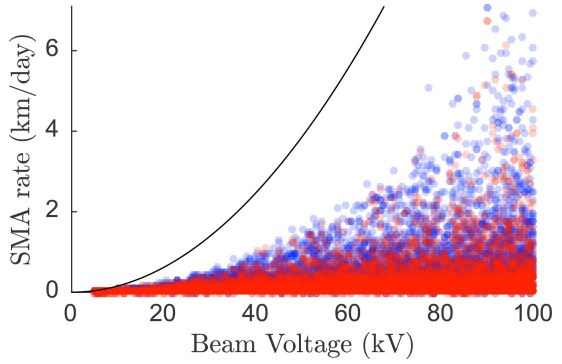

Fig. 6. Comparison of SMA rate produced by continuous (blue) and pulsed (red) electron beams. Theoretical maximum rate is shown as a solid black line.

force. This trend disappears in the upper plot due to the 100-kV beam voltage cap. As a comparison to prior work, the fastest SMA rate is near 6 km/day, which translates to reorbit times less than 2 months rather than the 2–4 month estimates in earlier work. As with the force analysis, the pulsed cases are consistently more efficient between 10 and 50 W.

To investigate a voltage-limited craft, the SMA rate is plotted against the beam voltage in Fig. 6.

The data once again have a quadratic bound, but this is not as striking a trend as the plot of force versus voltage in Fig. 4. This bound can be analytically predicted by combining the SMA rate equation, (8), the mass-to-radius relationship, (9), and the force optimum found earlier, (5). When this is done, the following SMA rate maximum is found:

$$\frac{\Delta a}{\text{day}} < \frac{4\pi}{n^2}\frac{F}{m} < \frac{4\pi}{n^2}\frac{0.00066350\frac{\text{m}}{\text{kg}}}{(R_D - 1.152)} \times \frac{4\pi\epsilon_0 R_T R_D}{80R_T^2 + 164R_T R_D + 80R_D^2} V^2. \quad (10)$$

The SMA rate is maximized when the deputy mass is low and the force is high. This is done by making the deputy as small as possible and making the tug and deputy the same size, which gives both of them a radius of 1.5 m. This explains why the quadratic boundary was not seen as clearly—the force maximum is found when both radii are equal while the SMA rate maximum requires both radii be equal and small. The quadratic boundary would likely become more evident if the number of Monte Carlo runs is increased. Inserting radii of 1.5 m for both craft yields the following theoretical bound for the SMA rate:

$$\frac{\Delta a}{\text{day}} < \left(1.5558 * 10^{-3}\frac{\text{km}}{\text{day kV}^2}\right) V^2. \quad (11)$$

For a beam of 100 kV, the maximum SMA rate is 15.58 km/day. This analytic maximum is shown as a black line in Fig. 6 and clearly bounds all data points.

VI. Equal Power Analysis

The Monte Carlo results show that if the beam voltage is limited and power is not, continuous beams always produce more force. However, if the beam power is limited and the voltage is not, pulsed beams can achieve higher forces if the power is low. This section uses deterministic equal power analysis to investigate the regions where pulsed beams produce more force than continuous beams.

A. Single Power Level

If our analysis is constrained to a certain power and tug and debris sizes, it changes the problem from 6-D to 3-D, two of which are nonphysical for continuous beams. To investigate the highest force produced at a single power level, small departures from optimal continuous beam cases are considered. The power in a beam for a continuous and pulsed beam is given by

$$P = I_{b_0} V_{b_0} = I_b V_b d \quad (12)$$

respectively, where a subsubscript of 0 indicates the continuous case. If both beams are constrained to have the same power, the pulsed voltage and current must rise, since $d < 1$. A way to raise both the voltage and the current equally is

$$I_b = \frac{I_{b_0}}{\sqrt{d}} \quad V_b = \frac{V_{b_0}}{\sqrt{d}}. \quad (13)$$

This deterministically allows for the effect of pulsing to be investigated in a 1-D manner. A degree of freedom is added to allow optimal tuning of the voltage and current

$$I_b = \frac{\gamma\, I_{b_0}}{\sqrt{d}} \quad V_b = \frac{V_{b_0}}{\gamma\sqrt{d}}. \quad (14)$$

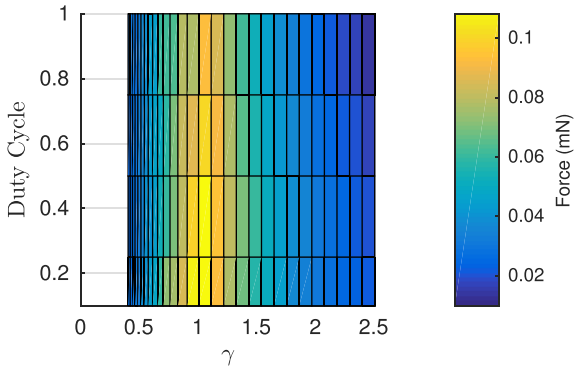

Fig. 7. Force produced at 16 W subject to changing voltage, current, and duty cycle.

A γ value greater than 1.0 indicates that current increases more than voltage, and a value below 1.0 indicates that voltage increases more than current. The pulse period was not found to make a large difference in the range of 0.1–1 s, so it is randomized and only the maximum force case is considered. This allows the problem to be analyzed deterministically in two dimensions.

In the following analysis, a 2-m tug and a 1.5-m deputy in nominal GEO space weather conditions separated by $\rho = 5(R_T + Rd) = 17$ m and a power of 16 W were considered. Continuous beam parameters are taken from Hogan [23] as $V_b = 37$ kV and $I_b = 432$ μA and produces a force of 0.2103 mN. Since the charging model used in this paper differs slightly, a 16-W optimum for continuous force is achieved at 23.9 kV and 670 μA. To expand this, the duty cycles of 10%, 25%, 50%, 75%, and the continuous case 100% are investigated. The voltage/current ratio tuning parameter γ varies logarithmically from 0.4 to 2.5, which gives equal space to look at high-voltage cases as high-current cases. A plot of the max force subject to the two deterministic parameters d and γ is shown in Fig. 7. Each row of this plot has the same duty cycle—the top row represents a continuous beam and the bottom row represents a pulsed beam with a 10% duty cycle. The columns of the plot have the same γ value, meaning that the relative scaling of voltage and current is the same, although both increase by $1/d$ as one travels up a column.

Equation (14) shows that current will be constant when $d \propto \gamma^2$. Since d is along the y-axis and γ is along the x-axis, parabolas are level curves in current in Fig. 7. Current is minimized in the bottom-right corner, maximized in the top-left corner, and steps up along ever-steepening parabolas between them. Level curves in voltage are given by $\gamma \propto (1/\sqrt{d})$, which in this plot translates to $y \propto 1/x^2$. Voltage is minimized in the bottom-left corner and maximized in the top-right.

The top row of Fig. 7 has a maximum at $\gamma = 1$, which confirms that the new values of 23.9 kV and 670 μA are optimal. The max force at lower duty cycles is also found with γ near 1, which gives a good starting point for optimizing the force. At this power level, the maximum average force produced by the pulsed beam is 23.8% larger than the maximum continuous force. In addition, a 10% duty cycle beam opens up 900-ms windows where both craft are uncharged and the beam is not operating. This would allow for small microthrust control maneuvers and measurements to be made without interference from the electron beam.

TABLE III
BASELINE CONTINUOUS BEAM PARAMETERS

Power (W)	V_{b0} (kV)	I_{b0} (mA)
2	7.9	0.253
4	11.4	0.351
8	17	0.471
16	29	0.552
32	41	0.781
64	57	1.123
128	79	1.620

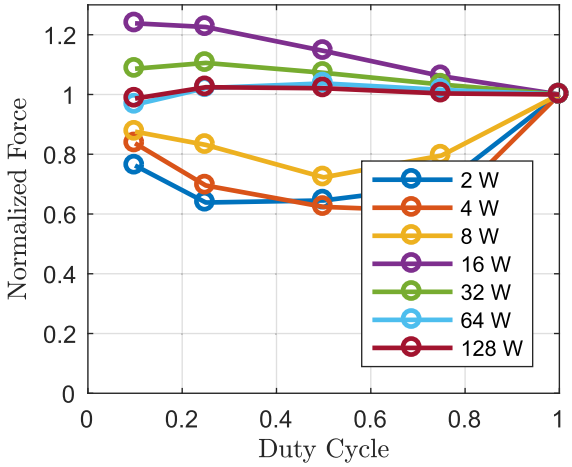

Fig. 8. Normalized force at different duty cycles for different power levels.

B. Power Level Range

To investigate whether the force increase persists at different power levels for these particular tug and debris object dimensions, this analysis is repeated at 2, 4, 8, 16, 32, 64, and 128 W. The baseline parameters (for the continuous case) are hand-tuned to find beam voltages within 1 kV of the optimal and are given in Table III. These baseline continuous voltages serve as starting points to ensure that the actual force maxima will lie within the γ range as is shown in Fig. 7.

If the maximum continuous force is treated as a baseline, the maximum average pulsed force can be compared by dividing the pulsed force by the continuous force. Values greater than 1 indicate situations where pulsing provides force benefits as well as windows of opportunity. This normalized force is shown as a function of the duty cycle in Fig. 8. Different power beams are shown as different color lines. For all powers above 8 W, there is a clear force benefit to pulsing—the average pulsed force is higher than the steady-state continuous force. The force increases are highest for 16 and 32 W, which is where previous work for the continuous ET has focused. This means that pulsing the beam that provides force efficiency

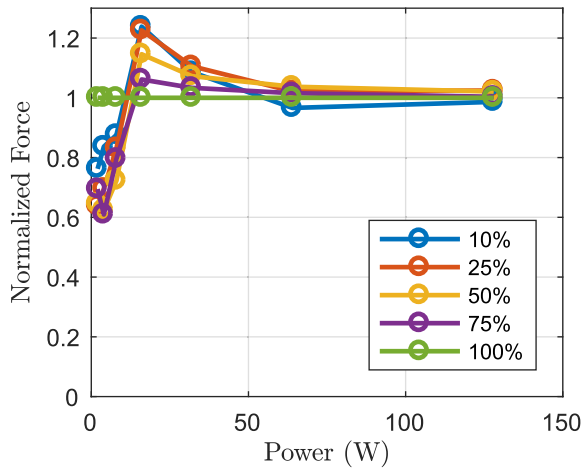

Fig. 9. Maximum force at a variety of duty cycles as a function of beam power.

increases as well as windows of opportunity in a relevant regime.

Note that the power levels at which the pulsed ET force magnitude advantages over the continuous ET solution are specific to the spacecraft dimensions assumed in this section. Differently sized objects would show a similar trend, but have distinct critical power levels.

These data can be visualized in a different way as well—plotting the normalized force against the power and using different lines for different duty cycles shows the power regime where pulsing is most beneficial. Each color in the plot in Fig. 9 represents a different duty cycle, with green being a continuous beam and blue being a 10% duty cycle. For the 2-, 4-, and 8-W beams, pulsing the beam actually decreases performance by between 10% and 40%. However, for all powers larger than 8 W, the average force with pulsing is higher. The largest gains occur at 16 W, and slowly drop to only a few percent improvements. The 10% duty cycle beam, although it has the greatest force increase at 16 W, performs worse than the continuous beam at 64 and 128 W. In addition, in all of these regimes, a pulsed beam offers 250–900-ms windows where both craft are discharged and the beam is not operating during which control maneuvers can be executed and measurements can be taken without beam interference.

VII. Conclusion

This paper introduces the pulsed ET and performs preliminary analysis to find regimes where it provides force increases. Six parameters (R_T, R_D, V_b, I_b, T_p, and d) are selected to vary in a Monte Carlo analysis. An analytic upper bound for the force between two spacecraft as a function of beam voltage is found, and has good agreement with the Monte Carlo results. In a voltage-limited case, continuous beams give more force. In a power-limited case, pulsed beams sometimes give more force. In this analysis, they can give up to 23% more force than continuous beams of the same power as long as the power is less than around 50 W. The results are then applied to orbit raising for both power and voltage-limited spacecraft. The pulsed ET is also more efficient for semimajor axis raising at low-power levels. A similar analytic upper bound for the semimajor axis rate as a function of beam voltage is found. This limit also has good agreement with the Monte Carlo results.

A deterministic equal power analysis is performed for continuous and pulsed beams at 2, 4, 8, 16, 32, 64, and 128 W for this particular spacecraft size and distance scenario. Force increases for a pulsed beam are found for all powers greater than 8 W, with the highest increases occurring at 16 W. Pulsing also opens up windows of opportunity to perform thrusting and take measurements at all power levels.

Pulsing the electron beam in the ET offers force increases for the same power in a certain power regime, and creates windows of opportunity during which control maneuvers can be executed and measurements can be taken without interference from the electron beam. This allows for faster reorbiting of GEO debris objects that are currently increasing the risk of collision in a very valuable orbital region.

Appendix
Charging Model

In this analysis, both spacecraft are subject to many environmental currents as well as a pulsed electron beam. The environmental currents are a function of the space plasma parameters and the voltage of the spacecraft (ϕ), and the electron beam is a function of time. The change in charge with time is the sum of the currents, which yields a forced ordinary differential equation for the charge on a spacecraft

$$\frac{dq}{dt} = I_{\text{beam}}(t)(1 - Y_B(E_L)) + I_e(\phi)(1 - < Y_e > (\phi)) + I_i(\phi)(1 + < Y_i > (\phi)) + I_p(\phi) \quad (15)$$

where the environmental currents considered are the electron and ion plasma current (I_e and I_i), and the photoelectric current (I_p). Electron currents (plasma and beam) are attenuated by SEE and backscattering, while the ion plasma current is increased by SEE. These effects are combined in the yields for the beam, electron current, and ion current (Y_B, Y_e, and Y_i). Each of these currents is described individually. The electron beam is typically chosen to be much larger than any other currents.

A. Electron Plasma Current

Electrons at GEO are tenuous and hot. The orbit motion limited method given by [17] is used to calculate the electron current

$$I_e = \begin{cases} -\dfrac{Aqn_e v_{\text{th}_e}}{4} e^{q\phi/k_B T_e}, & \phi < 0 \quad (16) \\ -\dfrac{Aqn_e v_{\text{th}_e}}{4}\left(1 - \dfrac{q\phi}{k_B T_e}\right), & \phi \geq 0 \quad (17) \end{cases}$$

where I_e is the electron plasma current [A], A is the spacecraft area [m^2], q is the fundamental charge [C], n_e is the electron density [#/m^3], and v_{th_e} is the electron thermal speed [m/s], which is given for either species by $v_{\text{th}} = (2k_B T/\pi m)^{1/2}$. The spacecraft voltage is ϕ [V], and $k_B T_e$ is the electron thermal energy [eV].

1) Electron-Induced SEE and Backscattering: When an electron impacts a material, it can impart some of its energy to the surrounding electrons, which may be ejected. These ejected electrons typically have very low energies (2 eV) but can cause a net current for a negative craft. The probability of a secondary electron being ejected is dependent on the landing energy of the incident electron and the angle of incidence. In this analysis, only normal incidence is considered. The dimensionless ratio of incoming incident electrons to outgoing secondary electrons as a function of landing energy is given by Lin and Joy [27]

$$\delta(E) = \delta_M 1.28 \left(\frac{E}{E_{\text{Me}}}\right)^{-0.67} \left(1 - e^{-1.614\left(\frac{E}{E_{\text{Me}}}\right)^{1.67}}\right). \quad (18)$$

Backscattering occurs when an electron is reflected from the spacecraft rather than absorbed. This analysis uses the model provided by the Nascap Scientific Documentation for energy-dependent backscattering [28]

$$\eta(E) = \left(\frac{H(1-E)H(E-0.05)\log\left(\frac{E}{0.05}\right)}{\log(20)} + H(E-1)\right) \times \left(\frac{e^{-E/5}}{10} + 1 - (2/e)^{0.037Z}\right) \quad (19)$$

where η is the dimensionless probability of backscattering, E is the landing energy in keV, $H(x)$ is the heaviside step function, and Z is the atomic number of the material (aluminum in this analysis). The formulas mentioned earlier can be added to produce the total yield $Y(E) = \eta(E) + \delta(E)$ for incident monoenergitic electrons.

B. Ion Plasma Current

The ion plasma current is a result of the ions impacting the spacecraft, absorbing an electron, and leaving the system. The model is similar to the electron plasma current with a polarity flip [17]

$$I_i = \begin{cases} -\frac{Aqn_i v_{\text{th}_i}}{4} e^{q\phi/k_B T_i}, & \phi > 0 \quad (20) \\ -\frac{Aqn_i v_{\text{th}_i}}{4}\left(1 - \frac{q\phi}{k_B T_i}\right), & \phi \le 0 \quad (21) \end{cases}$$

where v_{th_i} and $k_B T_i$ are the ion thermal speed [m/s] and thermal energy [eV], respectively. All ions are assumed to be protons. For both ions and electrons, the current absorbed from the attracted species at high potentials is approximately linear, and the current from the repulsed species exponentially decays with voltage.

C. Ion-Induced SEE

Ions may also cause SEE, and for many materials, the number of secondaries caused by ions is much larger than that caused by electrons. However, since the ion current is usually much smaller than the electron current, ion-induced SEE is neglected in many cases. For this application, where the spacecraft voltage exceeds the plasma temperature by an order of magnitude, ion-induced SEE must be considered.

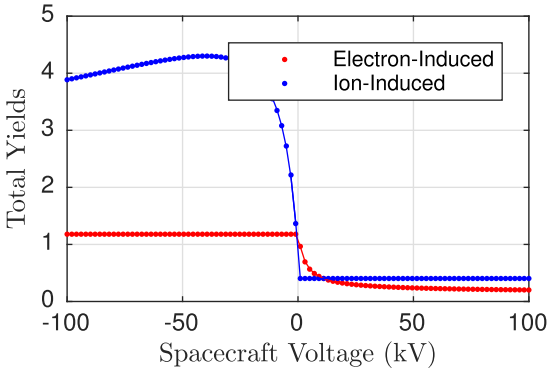

Fig. 10. Total yields for electrons and ions in representative GEO plasma.

In this analysis, the two-parameter Nascap model [28] is used

$$\delta(E) = \frac{\beta E^{1/2}}{1 + E/E_M}. \quad (22)$$

D. Total Yields

If the space plasma were monoenergetic, (18), (19), and (22) would be enough to form the total yields $\langle Y_e \rangle$ and $\langle Y_i \rangle$. However, space plasma is not monoenergetic, and in this analysis, a Maxwellian flux distribution is used

$$F(E) \propto E e^{-E/kT_e}. \quad (23)$$

The mean yield is found by integrating the product of the total yield and the current with respect to energy, and normalizing by the total current

$$\langle Y \rangle = \frac{\int_L^\infty Y(E)\, E \exp\left(-\frac{E \pm V}{kT}\right) dE}{\int_L^\infty E \exp\left(-\frac{E \pm V}{kT}\right) dE}. \quad (24)$$

For the $\pm$ and $\mp$ terms, the top sign is for the ions while the lower sign is for electrons. This integral is solved numerically using the u substitution $u = \exp(-(E \pm V)/kT)$ for the attracted species and $u = \exp(-E/kT)$ for the repulsed species. This transforms the integration domain from $E \in [L, \infty]$ to $u \in [0, 1]$. This is solved numerically using an iterative Gauss–Legendre quadrature-based integrator. This solver is chosen over simpler numeric integration schemes, such as Simpson's Rule or the Trapezoidal method, because it allows the user to specify the error tolerance. For this application, an error tolerance of 10^{-6} is used.

Using the electron and ion plasma temperatures given in Table I gives the plot shown in Fig. 10. In order to speed up computation, rational functions are used to fit the curves below rather than recomputing the yields at each time step. This produces the solid lines in Fig. 10 while performing the numeric integration gives the dots. The fits represent the numeric integrals well, with $R^2 = 0.9995$ for electrons and

TABLE IV
FITTING COEFFICIENTS FOR SEE AND BACKSCATTERING

Coefficients	Value	Coefficients	Value
p_{1E}	0.1748	q_{1E}	3.141
p_{2E}	3.808		
p_{1I}	1442	q_{1I}	255.5
p_{2I}	1689	q_{2I}	2001

$R^2 = 0.9997$ for ions. The fits are shown as follows:

$$\langle Y_e \rangle = \begin{cases} (p_{1E}V + p_{2E})/(V + q_{1E}), & V \geq 0 \\ 1.179, & V < 0 \end{cases}$$

$$\langle Y_e \rangle = \begin{cases} 0.403, & V \geq 0 \\ (-p_{1I}V + p_{2I})/(V^2 - q_{1E}V + q_{2I}), & V < 0 \end{cases}$$

where the voltage V is in kV. The parameters for the fit are shown in Table IV.

These fits are specific to aluminum spheres in the plasma specified in Table I. If the material or plasma is changed, these fits will no longer hold.

E. Photoelectron Current

Energy from the sun can energize electrons in the first few nanometers of the spacecraft surface so that they leave the surface. The fraction that have enough energy to escape the potential well of the spacecraft cause a net positive current given by [17]

$$I_p = \begin{cases} j_{\text{ph}} A_l e^{-q\phi/k_B T_{\text{ph}}}, & \phi > 0 \quad (25) \\ j_{\text{ph}} A_l, & \phi \leq 0 \quad (26) \end{cases}$$

where j_{ph} is the photoelectron flux [A/m^2], A_l is the illuminated area [m^2], and $k_B T_{\text{ph}}$ is the thermal energy of the ejected photoelectrons [eV]. For a negative spacecraft, this current is constant, and for a positively charged spacecraft, it quickly vanishes.

1) Electron Beam: If a beam of electrons is shot from the tug craft to the deputy craft, it will cause a positive current on the tug and a negative current on the deputy. If the beam does not have sufficient energy to escape the potential well of the tug, it will return and cause no net currents. If it has sufficient energy to leave the well of the tug, but insufficient energy to reach the deputy, the beam will diverge and disperse. These electrons have sufficient energy to escape the system, but some may impact the tug before they have a chance to escape. Further analysis is needed to quantify the fraction that does not escape, but in this analysis, it is assumed to be negligible. This is a good assumption, considering spacecraft with complex geometries and separation larger than radii. The currents on the debris are then given by

$$I_{\text{bd}} = \begin{cases} -I_b, & V_b > \phi_T - \phi_D \quad (27) \\ 0, & V_b < \phi_T - \phi_D \quad (28) \end{cases}$$

where I_{bd} is the beam current on the deputy [A], V_b is the accelerating voltage of the beam [V], and ϕ_t and ϕ_d are the potentials of the tug and deputy spacecraft, respectively. The currents on the tug are given by

$$I_{\text{bt}} = \begin{cases} I_b, & V_b > \phi_T \quad (29) \\ 0, & V_b < \phi_T - \phi_D. \quad (30) \end{cases}$$

2) Beam-Induced SEE: Since the beam is monoenergetic, the mean yield does not need to be computed. The landing energy is computed as

$$E_L = |q_e|(V_B - V_T + V_D) \quad (31)$$

and the SEE and backscattering coefficients can be evaluated directly as

$$Y_B(E_L) = \eta(E_L) + \delta(E_L) \quad (32)$$

without integrating over the flux distribution.

REFERENCES

[1] P. Chrystal, D. McKnight, P. L. Meredith, J. Schmidt, M. Fok, and C. Wetton, "Space debris: On collision course for insurers?" Swiss Reinsurance Company Ltd, Zürich, Switzerland, Tech. Rep. 1504360_11_en, Mar. 2011.

[2] P. V. Anderson and H. Schaub, "Local debris congestion in the geosynchronous environment with population augmentation," *Acta Astronautica*, vol. 94, no. 2, pp. 619–628, Feb. 2014.

[3] K. Wormnes *et al.*, "ESA technologies for space debris remediation," in *Proc. 6th IAASS Conf.: Safety Option*, Apr. 2013, pp. 3–4.

[4] P. Couzin, F. Teti, and R. Rembala, "Active removal of large debris: Rendez-vous and robotic capture issues," in *Proc. 2nd Eur. Workshop Active Debris Removal*, Paris, France, 2012, p. 7.5.

[5] Y. S. Karavaev, R. M. Kopyatkevich, M. N. Mishina, G. S. Mishin, P. G. Papushev, and P. N. Shaburov, "The dynamic properties of rotation and optical characteristics of space debris at geostationary orbit," *Adv. Astron. Sci.*, vol. 119, no. 4, pp. 1457–1466, Feb. 2004.

[6] C. Bombardelli and J. Pelaez, "Ion beam shepherd for contactless space debris removal," *J. Guid., Control, Dyn.*, vol. 34, no. 3, pp. 916–920, May 2011.

[7] S. Kitamura, "Large space debris reorbiter using ion beam irradiation," in *Proc. 61st Int. Astron. Congr.*, Prague, Czech Republic, Sep. 2010, pp. 1–27.

[8] D. F. Moorer, Jr. and H. Schaub, "Electrostatic spacecraft reorbiter," U.S. Patent 8 205 838 B2, Jun. 26, 2012.

[9] K. K. Galabova, "Architecting a family of space tugs based on orbit transfer mission scenarios," Ph.D. dissertation, Dept. Aeron. Astron., Massachusetts Inst. Technol., Cambridge, MA, USA, Feb. 2004.

[10] H. Schaub and D. F. Moorer, "Geosynchronous large debris reorbiter: Challenges and prospects," *J. Astron. Sci.*, vol. 59, no. 1, pp. 161–176, Jun. 2012.

[11] H. Schaub and Z. Sternovsky, "Active space debris charging for contactless electrostatic disposal maneuvers," *Adv. Space Res.*, vol. 53, no. 1, pp. 110–118, Jan. 2014.

[12] D. Stevenson and H. Schaub, "Rotational testbed for coulomb induced spacecraft attitude control," in *Proc. 5th Int. Conf. Spacecraft Formation Flying Missions Technol.* Munich, Germany, May 2013, pp. 27–31.

[13] T. Bennett, D. Stevenson, E. Hogan, L. McManus, and H. Schaub, "Prospects and challenges of touchless debris despinning using electrostatics," in *Proc. 3rd Eur. Workshop Space Debris Modeling Remediation*, Paris, France, Jun. 2014.

[14] D. Stevenson and H. Schaub, "Multi-sphere method for modeling electrostatic forces and torques," *Adv. Space Res.*, vol. 51, no. 1, pp. 10–20, Jan. 2013.

[15] T. Bennett and H. Schaub, "Touchless electrostatic three-dimensional detumbling of large geo debris," in *Proc. AAS/AIAA Spaceflight Mech. Meeting*, Jan. 2014, doi: 10.1007/s40295-015-0075-8.

[16] J. F. Fennell, H. C. Koons, M. S. Leung, and P. F. Mizera, "A review of SCATHA satellite results: Charging and discharging," Aerosp. Corp., El Segundo, CA, USA, Tech. Rep. TR-0084A(5940-05)-7, 1983, pp. 3–11.

[17] S. T. Lai, *Fundamentals of Spacecraft Charging: Spacecraft Interactions With Space Plasmas*. Princeton, NJ, USA: Princeton Univ. Press, 2011.

[18] C. Früh, D. C. Ferguson, C. Lin, and M. Jah, "The effect of passive electrostatic charging on near-geosynchronous high area-to-mass ratio objects," in *Proc. AAS Space Flight Mech. Meeting*, Santa Fe, NM, USA, Feb. 2014, paper AAS 14-428.
[19] W. E. Wiesel, "Estimating nongravitational accelerations on high area to mass ratio objects," *J. Guid., Control, Dyn*, vol. 39, no. 6, pp. 1438–1443, Feb. 2016.
[20] M. A. Peck, "Prospects and challenges for Lorentz-augmented orbits," in *Proc. Guid., Navigat. Control Conf. Exhibit*, San Francisco, CA, USA, Aug. 2005, pp. 15–18.
[21] M. A. Peck, B. Streetman, C. M. Saaj, and V. Lappas, "Spacecraft formation flying using Lorentz forces," *J. Brit. Interplanetary Soc.*, vol. 60, pp. 263–267, Jul. 2007.
[22] B. Streetmann and M. A. Peck, "Gravity-assist manuvers augmented by the Lorentz force," *J. Guidence, Control, Dyn*, vol. 32, no. 5, pp. 1639–1647, Sep. 2009.
[23] E. A. Hogan, "Impacts of tug and debris sizes on electrostatic tractor charging performance," *Adv. Space Res.*, vol. 55, no. 2, pp. 630–638, Jan. 2015.
[24] E. A. Hogan and H. Schaub, "Impacts of hot space plasma and ion beam emission on electrostatic tractor performance," *IEEE Trans. Plasma Sci.*, vol. 43, no. 9, pp. 3115–3129, Sep. 2015.
[25] M. H. Denton, M. F. Thomsen, H. Korth, S. Lynch, J. C. Zhang, and M. W. Liemohn, "Bulk plasma properties at geosynchronous orbit," *J. Geophys. Res.: Space Phys.*, vol. 110, no. A7, Jul. 2005. [Online]. Available: http://dx.doi.org/10.1029/2004JA010861
[26] E. A. Hogan and H. Schaub, "Space weather influence on relative motion control using the touchless electrostatic tractor," in *Proc. AAS/AIAA Spaceflight Mech. Meeting*, Jan. 2014.
[27] Y. Lin and D. C. Joy, "A new examination of secondary electron yield data," *Surf. Interface Anal.*, vol. 37, no. 11, pp. 895–900, Nov. 2005.
[28] V. A. Davis and M. J. Mandell, *Plasma Interactions With Spacecraft. Volume 2, NASCAP-2K Scientific Documentation for Version 4.1*, 4th ed. San Diego, CA, USA: Science Applications International Corp., 2011.
[29] E. Hogan and H. Schaub, "Space weather influence on relative motion control using the touchless electrostatic tractor," *J. Astron. Sci.*, vol. 63, no. 3, pp. 237–262, Sep. 2016.
[30] W. R. Smythe, *Static and Dynamic Electricity*, 3rd ed. New York, NY, USA: McGraw–Hill, 1968.
[31] D. J. Griffiths, *Introduction to Electrodynamics*, 4th ed. Englewood Cliffs, NJ, USA: Prentice Hall, 1999.
[32] N. Murdoch, D. Izzo, C. Bombardelli, I. Carnelli, A. Hilgers, and D. Rodgers, "Electrostatic tractor for near earth object deflection," in *Proc. 59th Int. Astron. Congr.*, Glasgow Scotland, U.K., 2008, paper IAC-08-A3.I.5.
[33] C. R. Seubert, L. A. Stiles, and H. Schaub, "Effective coulomb force modeling for spacecraft in earth orbit plasmas," *Adv. Space Res.*, vol. 54, no. 2, pp. 209—220, Jul. 2014.
[34] H. Schaub and L. E. Z. Jasper, "Orbit boosting maneuvers for two-craft coulomb formations," *J. Guid., Control, Dyn.*, vol. 36, no. 1, pp. 74–82, Jan./Feb. 2013.
[35] D. Schrage, *et al.*, "A flight-qualified RFQ for the bear project," in *Proc. Linear Accelerator Conf.*, Williamsburg, VA, USA, Oct. 1988, pp. 54–57.
[36] P. G. O'Shea, T. Butler, M. Lynch, K. McKenna, M. Fongratz, and T. Zaugg, "A linear accelerator in space–the beam experiment aboard rocket," in *Proc. Linear Accelerator Conf.*, Albuquerque, NM, USA, Sep. 1990, pp. 739–742.
[37] R. Harris, *Modern Physics*. Pearson, India, 1998.
[38] B. Macomber, D. Conway, K. A. Cavalieri, C. Moody, and J. L. Junkins, "Lasr cv: Vision-based relative navigation and proximity operations pipeline," in *Proc. Adv. Astron. Sci., Guidence, Navigat., Control*, vol. 151, 2014.
[39] D. Matko *et al.*, "Validation of astrodynamic formation flying models against space-si experiments with prisma satellites," in *Proc. 26th Annu. Conf. Small Satellites*, Logan, UT, USA, 2012, paper SSC12-II-2.

Authors' photographs and biographies not available at the time of publication.